

Article

Strain Hardening Behavior and Microstructure Evolution of High-Manganese Steel Subjected to Interrupted Tensile Tests

Adam Grajcar *, Aleksandra Kozłowska and Barbara Grzegorzczuk

Faculty of Mechanical Engineering, Silesian University of Technology, 18a Konarskiego Street, 44-100 Gliwice, Poland; aleksandra.kozlowska@polsl.pl (A.K.); barbara.grzegorzczuk@polsl.pl (B.G.)

* Correspondence: adam.grajcar@polsl.pl; Tel.: +48-32-237-2933

Received: 18 January 2018; Accepted: 7 February 2018; Published: 10 February 2018

Abstract: Strain hardening behavior and the corresponding microstructure evolution of the high-manganese steel with additions of Si and Al were investigated in this study. Thermomechanically processed and solution-heat-treated sheet steels were compared under conditions of interrupted tensile tests. Relationships between microstructure and strain hardening were assessed for different strain levels using light microscopy and scanning electron microscopy techniques. It was found that the deformation of both steels at low strain levels was dominated by dislocation glide before the occurrence of mechanical twinning. The amount of twins, slip lines, and bands was increasing gradually up to the point of necking. As the strain level increased, dislocation density within twinning areas becomes higher, which enhances the strength, the work hardening exponent, and the work hardening rate of the investigated high-manganese sheet steels.

Keywords: strain hardening; microstructure; twinning; interrupted tensile test; high-Mn steel

1. Introduction

A beneficial strain hardening behavior of high-manganese steels depends significantly on the extent of TRIP (Transformation Induced Plasticity) and TWIP (Twinning Induced Plasticity) effects. These phenomena can take place both at a forming stage or later during an exploitation stage [1,2]. High-manganese steels are characterized by a pure austenitic microstructure due to a manganese content ranging typically between 20% and 30% [3–5]. A stimulation of mechanical and other properties can be done using various combinations of Al, Si, Cr, and N. These steels are strengthened due to a complex interaction of dislocation glide, mechanical twinning, and α/ϵ martensite formation. The martensite platelets and mechanical twins act as obstacles to dislocation motion and block the movement of dislocations, and in this way they affect the work hardening behavior of high-manganese steels. The mentioned microstructural effects determine the mechanical behavior of steel, resulting in the delay of local necking, which allows for large uniform elongations [6–11].

A type of the deformation mode depends on a chemical composition of steel and temperature and strain rate. It is related to stacking-fault energy (SFE) of the austenite. With increasing SFE, the mechanisms change from a martensitic transformation (occurs when SFE is lower than 25 mJ/m²) to a mechanical twinning (SFE in a range of 25–60 mJ/m²). If SFE value is higher than 60 mJ/m², the steel is strengthened mostly by the dislocation glide [12]. The strengthening process is also strongly related to grain size [13–16]. Yuan et al. [17] reported that deformation twins form easily during tensile deformations when initial grain size increases. The effect of grain size on the mechanical properties of their steels was also detected—the yield and ultimate tensile strengths decrease with the increase in grain size, while the elongation increases. Dini et al. [18] reported that in TWIP steels the onset of mechanical twinning shifts to a lower strain as grain size increases. Moreover, they noted that, during

tensile stresses, the occurrence of mechanical twins increases with increasing strain, meaning that the work hardening increases due to the presence of mechanical twin boundaries (the dynamic Hall-Petch effect). Unfortunately, fatigue resistance of coarse-grained microstructures is lower than fine-grained steels [19].

A chemical composition of steel affects the SFE. Aluminum addition strongly increases SFE, whereas silicon causes an opposite effect. Park et al. [20] reported that, regardless of the SFE and/or the Al content, deformation was achieved by planar glide of dislocations before mechanical twinning occurred. The planar glide became more evident as the SFE increased by suppressing or delaying mechanical twinning. As the SFE is increased by Al addition, the critical stress for initiation of the mechanical twinning becomes higher [20]. It was also reported [21,22] that Al additions lead to a lower strain hardening rate and decrease the frequency of mechanical twins formation, resulting in a decrease in tensile strength. Allain et al. [23] noted that the addition of approximately 3 wt % Si to high-Mn TWIP steel has a remarkable effect on dislocation mobility by significantly reducing the activation volume and mean free path, affecting the yield strength and work-hardening rate. Pierce et al. [24] indicated that manganese addition significantly affects the SFE. Strength and ductility decrease when the SFE is higher than 39 mJ/m² corresponding to a reduction in mechanical twinning.

Usually, the strain hardening behavior is reported for the whole deformation extent. A very limited number of papers addressed the microstructure evolution and corresponding progressive work hardening response of high-manganese steels during an interrupted tensile test. Therefore, the goal of the current study is to link the microstructure—mechanical property relationships of the microalloyed high-Mn steel containing additions of Si and Al.

2. Materials and Methods

The investigations were carried out on X4MnSiAlNbTi27-4-2 type steel, which belongs to the second generation of advanced high strength steels (AHSS). Table 1 shows the chemical composition of the investigated material.

Table 1. Chemical composition of investigated steel in wt %.

C%	Mn%	Si%	Al%	S%	P%	Nb%	Ti%	N%	O%
0.040	27.50	4.18	1.96	0.017	0.004	0.033	0.010	0.0028	0.0007

The investigated steel was melted in a vacuum furnace (VSB 50 Balzers, Asslar, Germany). After melting and casting, the ingot was hot-forged and roughly hot-rolled in a temperature range between 900 and 1200 °C to a thickness of ca. 4.5 mm. Then, the sheet was hot-rolled in three passes to a final thickness of 2 mm (obtained at 850 °C). Next, the samples were cooled in water to room temperature.

Two groups of samples were prepared (Figure 1):

1. Thermomechanically processed;
2. Thermomechanically processed and annealed at 900 °C within 20 min.

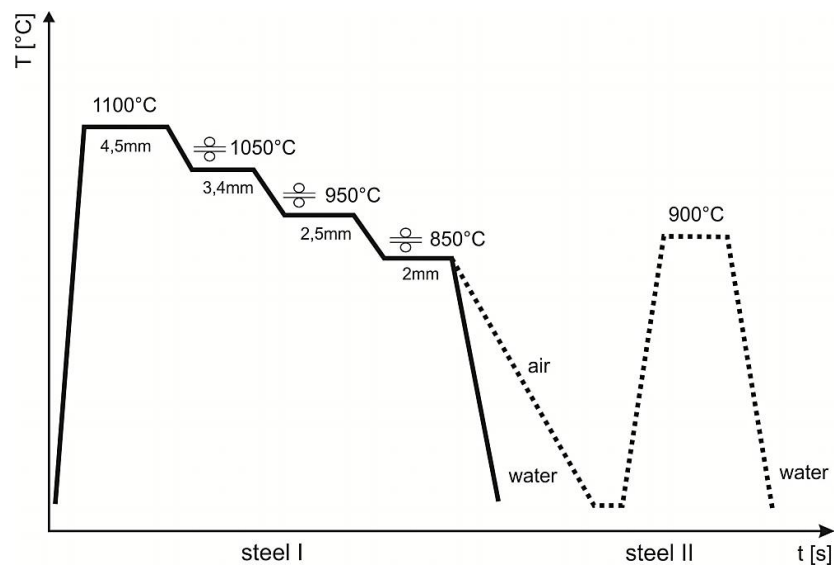


Figure 1. Parameters of thermomechanical processing to obtain hot-rolled steel (Steel I) and solution-heat-treated steel (Steel II).

The detailed conditions of the hot rolling are listed in Table 2.

Table 2. Conditions of the thermomechanical rolling.

Pass Number	Deformation Temperature (°C)	Sheet Thickness before a Pass (mm)	Sheet Thickness after a Pass (mm)	Absolute Reduction (mm)	Relative Strain (%)	Strain Rate (s ⁻¹)
1	1050	4.5	3.4	1.1	25	8.3
2	950	3.4	2.5	0.9	25	10
3	850	2.5	2.0	0.5	20	10

Room temperature uniaxial tensile tests were performed using 2 mm thick samples machined from the thermomechanically rolled sheet in the rolling direction. Tensile tests were interrupted at defined strain values of 5%, 10%, and 20% and at a final rupture at a strain rate of $5 \times 10^{-3} \text{ s}^{-1}$. The test was performed to monitor the microstructure evolution at the different strain levels. Based on results of the tensile tests, the yield stress (YS), tensile strength (UTS), and uniform and total elongation were determined. Moreover, the work hardening rate and the work hardening exponent n were calculated.

Polished with Al_2O_3 and etched using 5% Nital, samples were optically examined after the samples were deformed to predetermined strain levels. The specimens for optical observation were taken from the middle of the deformed specimen length, according to the tensile direction. The optical observations were performed using a Zeiss Axio Observer Z1m optical microscope (Carl Zeiss AG, Jena, Germany). Detailed microstructure analysis was performed using a scanning electron microscope Zeiss SUPRA 25 (Carl Zeiss AG, Jena, Germany) operating at 20 kV.

3. Results and Discussion

3.1. Initial Material

An optical micrograph of the thermomechanically processed sample in the initial state is shown in Figure 2a. The occurrence of annealing twins inside austenite grains elongated in the direction of hot rolling can be observed. The microstructure is relatively coarse-grained due to relatively low deformation levels; the average grain size was estimated to be about 70 μm . Elongated sulfide inclusions were also observed. Figure 2b shows the micrograph of a hot-rolled

and subsequently solution-heat-treated specimen. The microstructure is characterized by a more fine-grained microstructure due to a relatively low annealing temperature. The average grain size was estimated to be about 37 μm .

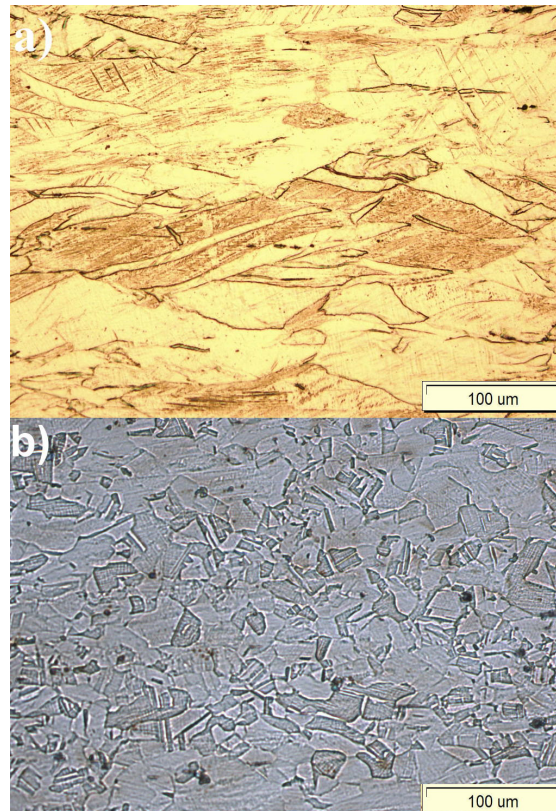


Figure 2. Austenitic microstructures of (a) thermomechanically rolled steel and (b) solution-heat-treated steel.

3.2. Microstructure Changes during Interrupted Tensile Tests

Steel samples were subjected to interrupted tensile tests at different strain levels of 5%, 10%, and 20% and at the point of rupture. Microstructure evolution was observed at each deformation step. Figure 3a,b show that the samples deformed up to a 5% strain. Slip lines and bands were observed both in the microstructure of thermomechanically processed and solution-heat-treated steels. No deformation twins were observed (Figure 4a,b). Dislocation activity always occurs before the twinning mechanism [20,25]. The twinning deformation will start when the stress concentration, which is provided by piled-up dislocations, surpasses the critical stress for deformation twins [21]. The stress needed for twins to nucleate is far more than that for twins to grow [25]. Park et al. [20] reported that in Fe-22Mn-0.6C solution-heat-treated steel, from the initial stage of deformation (5%), mechanical twinning occurred and its population continuously increased with increasing strain. They indicated that planar glide dominated deformation before the activation of mechanical twinning for all investigated steels regardless of the SFE. Mazurkiewicz [26] observed the dominant character of slip lines in X8MnSiAlNbTi25-1-3 steel deformed up to 10%. The mechanical twins were observed at higher deformation levels—above 20%. We also observed that the dislocation glide occurs at a lower deformation level, before twinning initiation.

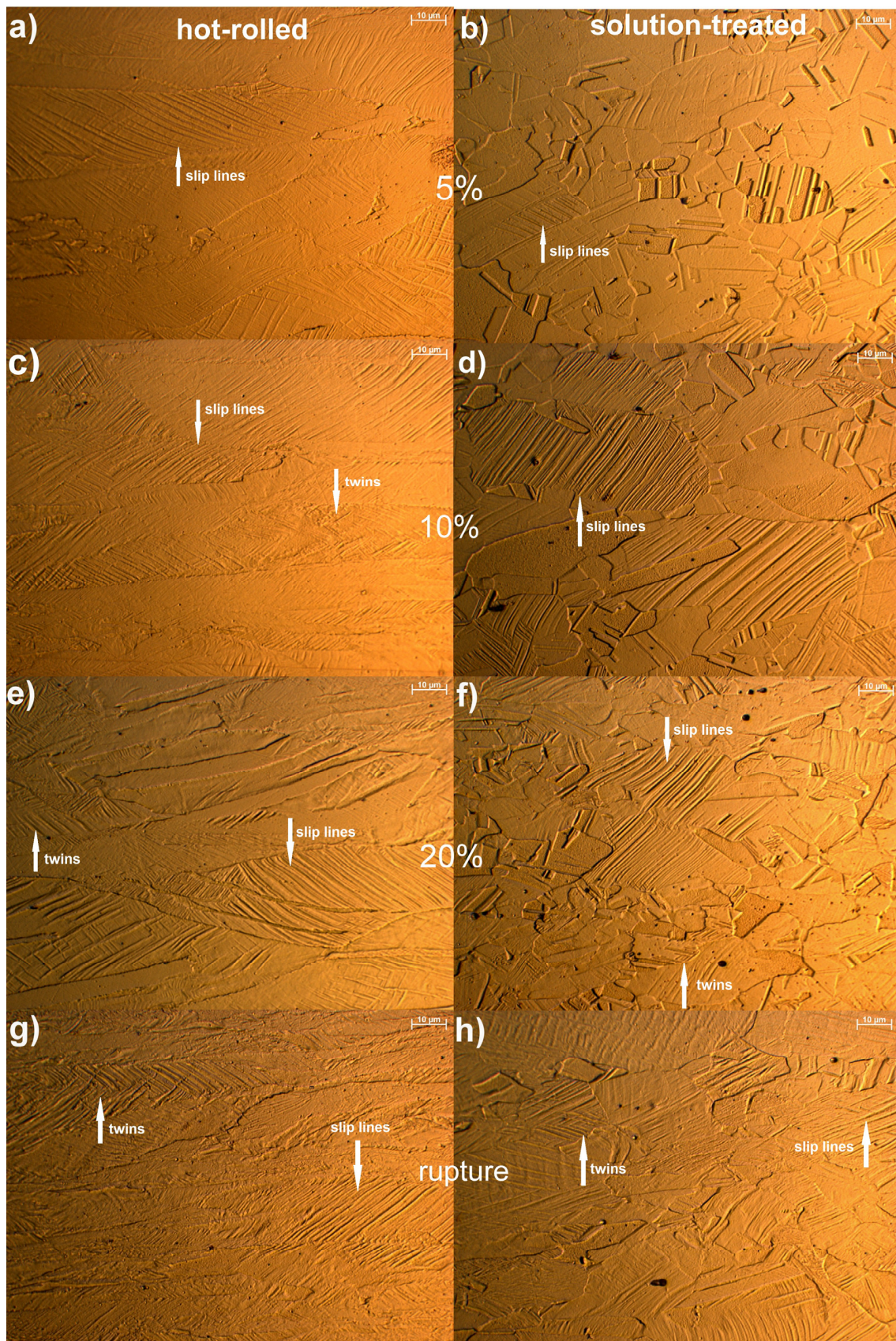


Figure 3. Microstructures of the investigated steel deformed at 5% (a,b), 10% (c,d) and 20% (e,f) strain levels and at the point of rupture (g,h).

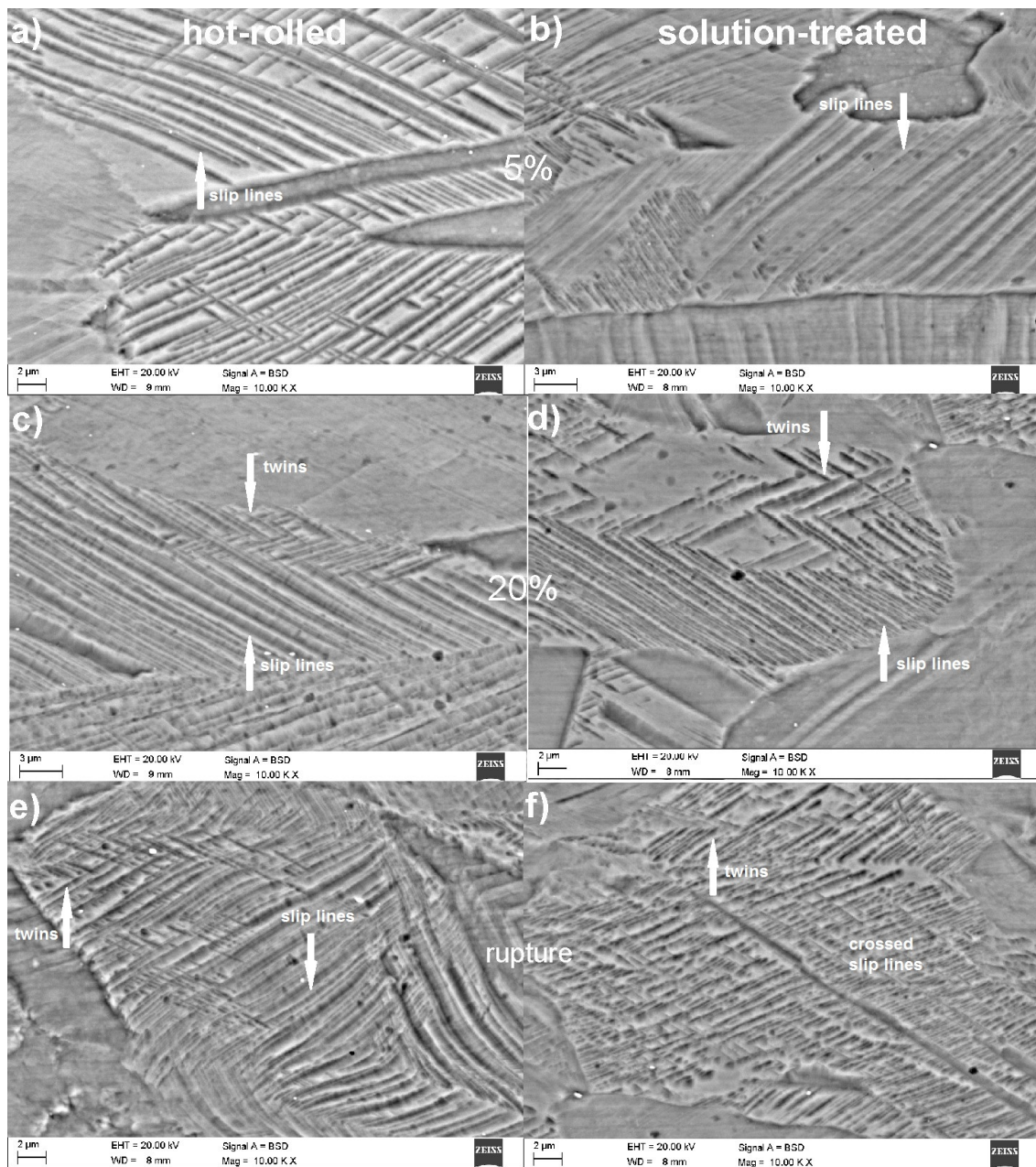


Figure 4. Scanning electron microscope (SEM) images of the investigated steel deformed at 5% (a,b) and 20% (c,d) strain levels and at rupture (e,f).

The microstructures of the investigated steels strained to 10% (Figure 3c,d) are characterized by austenite grains elongated according to the stretching direction. The grains are more elongated in the case of hot-rolled steel. The presence of numerous crossed deformation lines and bands was revealed in both hot-rolled and solution-heat-treated steel. Moreover, single mechanical twins were observed in the hot-rolled specimen. Park et al. [20] reported that, in solution-heat-treated Fe-0.6C-22Mn-3Al steel, the mechanical twins were observed at 10% strain, whereas in Fe-0.6C-22Mn-6Al steel twins appeared at high strains over 40%. This indicates that Al addition strongly increases the SFE, resulting in the retardation of twinning occurrence. Peng et al. [21] observed in Fe-1.3C-20Mn TWIP steel that a large number of mechanical twins at 11% strain. However, mechanical twins were not observed in the Fe-1.3C-20Mn-3Cu TWIP steel. The twinning mechanism occurred in this case at 20% strain. This was due to the higher SFE of the steel with Cu addition. The occurrence of twinning is strongly

related to the SFE, which depends on the chemical composition of steel. Aluminum concentrations in the steel investigated in the present work are close to those reported by Park et al. [20]. Hence, the strain level needed to activate the twinning mechanism was similar: 10% and 11%, respectively. Ghasri-Khouzaen et al. [27] investigated the relationship between strengthening mechanisms and carbon content in Fe-0.6C-22Mn steels. They found that the deformation products were mechanical twins for the 0.6C alloy and ϵ -martensite for the 0C and 0.2C alloys. For the 0.4C alloy, both mechanical twins and ϵ -martensite were identified during deformation.

An increase in the deformation level to 20% results in an increase in the amount of deformation twins in the thermomechanically rolled steel (Figures 3e and 4c). Moreover, deformation twins occur in the solution-heat-treated specimen (Figures 3f and 4d). The amount of deformation twins is higher in the hot-rolled steel when compared to the solution-heat-treated sample. Crossed deformation lines, bands, and twins were also observed. Twin population continuously increased with increasing strain from 10% to 20%.

Deformation twins are nucleated preferentially at grain boundaries, which act as sources for stacking faults. Most grains develop one main twinning system in addition to the dislocation glide. In TWIP steels, long primary twins often occur and span a grain from one grain boundary to another. Secondary twins may be nucleated within the twins of the primary system [28]. Wang et al. [29] observed the microstructure evolution in 316 stainless steel in a range of deformation levels: 10–30%. Deformation features evolved from planar dislocations to a single system twinning, then to multi-system twinning and intersections among twins, with increasing strain. Ding et al. [25] reported that, for deformation strains between 0.35 and 0.45, crossed twins occurred. Moreover, martensite transformation $\epsilon \rightarrow \alpha$ occurred at the place of these crossed twins, and martensite grew along the thickness of the twinned regions. No martensites ϵ or α' were observed in the investigated microstructure (Figures 3a–h and 4a–h). It was confirmed in our earlier research using X-ray diffraction [8]. Such behavior is typical for steels characterized by an SFE >20 mJ/m², resulting from the chemical composition.

Samples deformed to rupture are characterized by numerous crossed slip lines and bands (Figure 3g,h). The amount of crossed slip lines, bands, and deformation twins is higher than in the samples deformed to smaller deformation levels (Figure 4e,f). Intensively elongated austenitic grains are visible in the case of the thermomechanically rolled sample (Figure 3g). The grain size of this austenitic steel has a great effect on the formation and morphology of deformation twins. With the increase in grain size, deformation twins become easier to form. Yuan et al. [17] reported that deformed tensile samples with a grain size of 2.2 μm showed no deformation twins. In contrast, in samples with a grain size of 5.4–28.7 μm , deformation twins were easily found. Dini et al. [18] proved that in TWIP steels the onset of mechanical twinning shifts to a lower strain as grain size increases. In our case, for the solution-heat-treated steel, average grain size was estimated to be about 37 μm (Figure 2b), whereas the average grain size of hot-rolled steel was about 70 μm (Figure 2a). As mentioned before, a coarse-grained microstructure enhanced the occurrence of mechanical twins, so mechanical twins nucleated at lower strain levels in the case of the hot-rolled steel.

3.3. Strain Hardening Behavior

The interrupted tensile tests were performed at strain levels of 5%, 10%, 20% and at rupture in order to identify deformation-induced strengthening mechanisms. Mechanical properties of the hot-rolled steel were compared to the solution-heat-treated steel. The results of the tensile tests are shown in Table 3. The thermomechanically processed steel shows higher UTS and TE values (808 MPa and 44.8%, respectively) when compared to the solution-heat-treated specimen (727 MPa and 29.5%, respectively). The hot-rolled steel shows a YS/UTS ratio ca. 0.68, which indicates its relatively high strengthening potential. The solution-heat-treated specimen shows a lower YS/UTS ratio (0.59) due to the lower yield stress (it is lower by above 100 MPa). However, the more fine-grained microstructure results in its lower ultimate tensile strength because of the hampering effect of the smaller grain size on twin formation. The hot-rolled steel is also characterized by higher uniform elongation (UE) due to the

more coarse-grained microstructure. The same effect was observed by Yuan et al. [17]. Yield stress (YS) values were determined at each deformation level (Table 3). Generally, the thermomechanically rolled steel shows a higher YS than the solution-heat-treated steel due to the higher dislocation density after hot rolling. The microstructure of the steel after solution heat treatment contains a smaller dislocation density and finally a smaller YS value.

Table 3. The mechanical characteristics of the investigated steels.

Steel Type	UTS (MPa)		YS (MPa)			YS/UTS	UE (%)	TE (%)
Deformation level	-	5% 10% 20%	Max.	Average value		-	-	-
Hot-rolled	808	550 530 600	550	557		0.68	26.7	44.8
Solution-heat-treated	727	433 440 420	428	430		0.59	23.7	29.5

Curves showing true stress vs. true strain, work hardening exponent vs. true strain, and strain hardening rate vs. true strain are presented in Figures 5–7, respectively. Each curve terminates at a maximum uniform elongation. Figure 5 shows the true stress vs. true strain curves obtained at different strain levels. Both steels showed continuous and gradual strain hardening, typical for high-manganese TWIP steels [30–32]. Necking strains (corresponding to uniform elongation) obtained for the hot-rolled and solution-heat-treated steels were 0.24 and 0.21, respectively (Figure 5d).

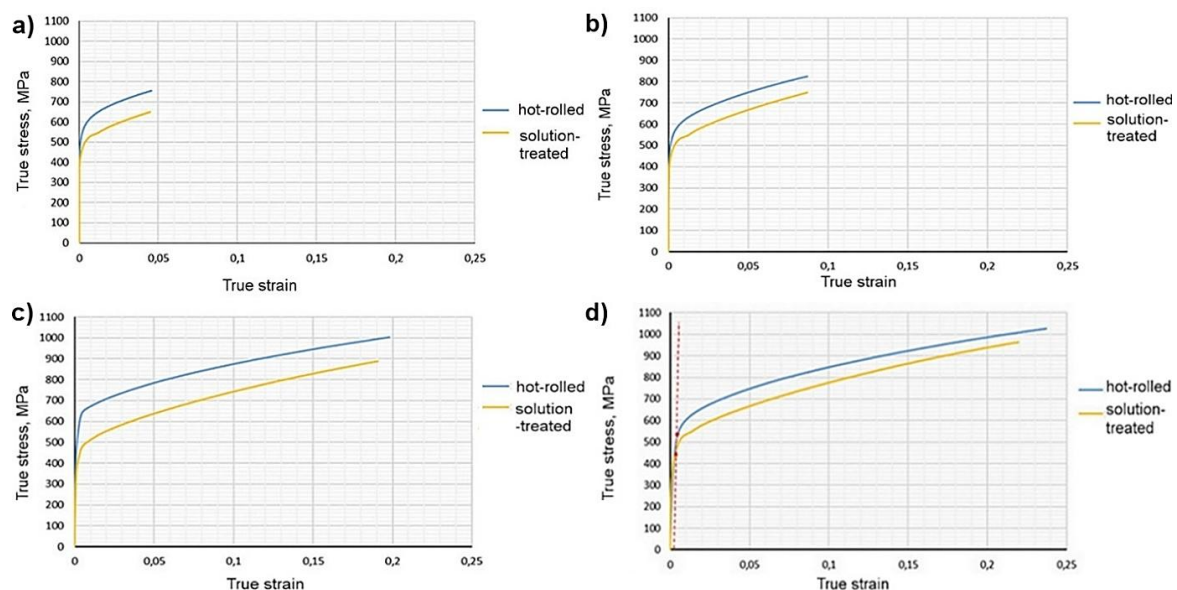


Figure 5. True stress–true strain curves of thermomechanically rolled and solution-heat-treated steels at different deformation levels of (a) 5%, (b) 10%, and (c) 20% and at (d) rupture.

In the case of the hot-rolled steel, the n exponent increases gradually to a maximum value of 0.24 corresponding to the true strain ~ 0.2 (Figure 6). Then, it decreases up to the point of necking. A slope of the n vs. true strain curve is lower in the case of the hot-rolled steel. This means that the steel is strengthened in a gradual way. Finally, it is reflected in a higher uniform elongation. The solution-heat-treated steel is characterized by a higher rate of strain hardening. That is why the n exponent increases intensively up to 0.33 at the true strain ~ 0.17 ; then, the n exponent rapidly decreases up to the point of necking (Figure 6), which is related to the difficult activation of the enhanced twinning in a fine-grained steel.

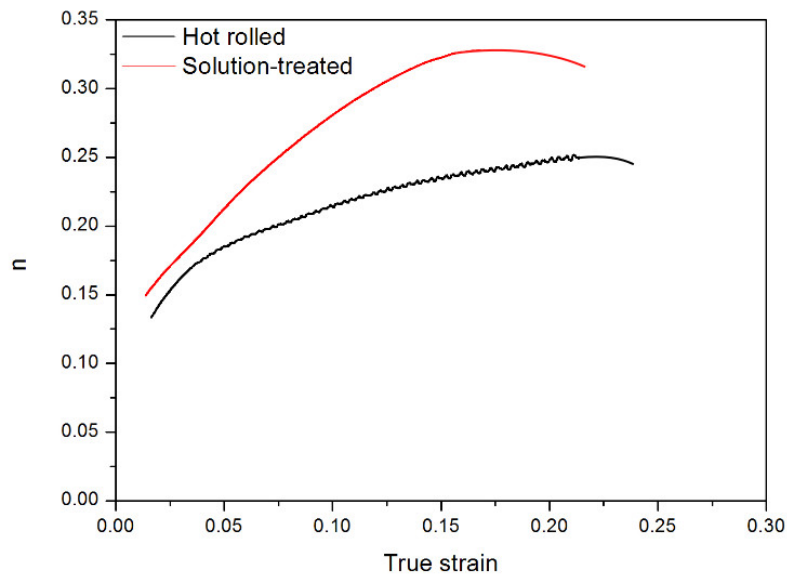


Figure 6. Work hardening exponent as a function of true strain.

Microstructural changes are reflected in the work hardening behavior of the investigated steels. A progressive character of the twinning mechanism allows for large uniform elongation in combination with the high tensile strength. The hot-rolled steel showed a greater tendency to twinning than the solution-heat-treated steel, so higher uniform elongation and better strength properties were obtained in this case (Table 3). Xie et al. [31] observed that the interactions between dislocations and twin boundaries introduced by prior cold-drawing of 316 austenitic stainless steel may benefit the deformation uniformity and delay the initiation of fatigue cracking. Liu et al. [32] reported that the work hardening behavior depends also on strain state. They reported that the strength and failure strain in tension of the Fe-20Mn-1.2C are higher than those obtained for the rolling and shear states. This was due to the higher twinning volume fraction in the case of tension stresses. Under tensile deformation, twinning tends to be initiated in grains with the $\langle 111 \rangle$ orientation in the tensile direction [28].

As can be seen in Figure 7, the $d\sigma/d\varepsilon$ values decrease rapidly at the initial range of deformation; then, the work hardening rate stabilizes at a constant level due to the combined occurrence of deformation twinning and deformation slip. The strain hardening rate of the thermomechanically rolled and solution-heat-treated steels rapidly decreased up to a true strain of ~ 0.04 and then decreased monotonically down to ~ 1500 MPa. Liu et al. [32] reported that effects of twinning on strain hardening become dominant when the twinning volume fraction reaches about 5% and evidently increases with increasing strain. Therefore, the relative stability of the strain hardening rate above true strain ~ 0.04 is probably related to the increase in twin volume fraction. As the deformation level increases, the dislocation density in the twinning areas becomes higher [20], which can promote the strength (Figure 5), the strain hardening exponent (Figure 6), and the strain hardening rate (Figure 7) of the investigated materials. It was reported [19,28,33] that the strain hardening of high-Mn TWIP steels is controlled via the dynamic Hall-Petch mechanism. The formation of twins gradually reduces the dislocation mean free path, increasing fragmentation of the grains via twin lamellae and finally contributing to enhanced dislocation storage and the subsequent work hardening rate. Bouaziz et al. [33] concluded that, of all possible deformation mechanisms in TWIP steels, deformation twinning had the most beneficial effect on strain hardening. The shape of the curves is very similar up to a true strain of ~ 0.08 . The work strengthening rate of the solution-heat-treated specimen was slightly higher over a strain range of 0.1–0.2. An enhanced strengthening leads to a faster blocking of the dislocation–twinning interactions, leading to faster neck initiation and resulting in lower uniform and total elongations. A more gradual change in the work hardening rate is more beneficial for obtaining a better balance of ductility and strength for the thermomechanically processed steel.

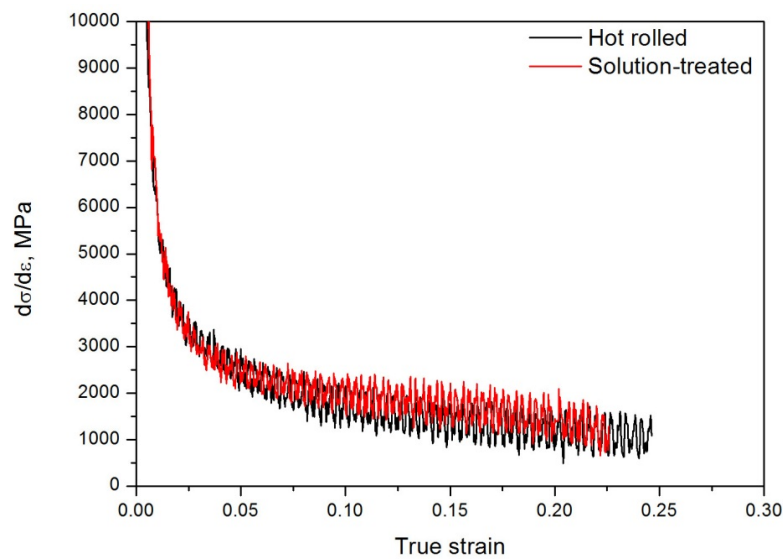


Figure 7. Work-hardening rate as a function of true strain.

4. Conclusions

The relationships between the strain hardening behavior and corresponding microstructure evolution during interrupted tensile tests for thermomechanically processed and solution-heat-treated high-manganese steels containing increased amounts of Si and Al were determined. It was found that the progress of work strengthening is controlled by the combination of dislocation slip and deformation twinning. The dislocation slip occurred before twinning at a lower strain level. The twinning was activated at strain levels ca. 10% and 20% correspondingly for the thermomechanically rolled and solution-heat-treated steels. The amount of deformation twins and slip bands increased gradually up to the point of necking for the hot-rolled steel, whereas the increase in deformation effects was faster for the solution-heat-treated steel with a smaller initial grain size. The twinning was enhanced for the coarse-grained microstructure because the twins nucleated at a lower strain level for the hot-rolled steel, bringing a better product of strength and ductility. Further research is needed to complete microscopic observations by Transmission Electron Microscopy and Electron Back-Scattered Diffraction results. The strain hardening rate of both investigated steels rapidly decreased up to a true strain of ca. 0.04 and then decreased monotonically due to the complex interaction of deformation twinning and dislocation slip. The more gradual progress of the strengthening of the thermomechanically processed steel leads to higher mechanical properties.

Acknowledgments: This work was financially supported with statutory funds of the Faculty of Mechanical Engineering of Silesian University of Technology in 2018.

Author Contributions: A.G. conceived, designed, and performed the experiments; A.K. performed the work hardening calculations, analyzed the corresponding results, and wrote the paper; B.G. linked the relationships between microstructure and work hardening behavior, analyzed the data, and reviewed the paper.

Conflicts of Interest: The authors declare no conflict of interest.

References

1. Mesquita, R.A.; Schneider, R.; Steineder, K.; Samek, L.; Arenholz, E. On the austenite stability of a new quality of twinning induced plasticity steel, exploring new ranges of Mn and C. *Metall. Mater. Trans. A* **2013**, *44*, 4015–4019. [[CrossRef](#)]
2. Kuc, D.; Hadasik, E.; Niewielski, G.; Schindler, I.; Mazancova, E.; Ruz, S.; Kawulok, P. Structural and mechanical properties of laboratory rolled steels high-alloyed with manganese and aluminium. *Arch. Civ. Mech. Eng.* **2012**, *12*, 312–317. [[CrossRef](#)]

3. Grajcar, A.; Kuziak, R. Softening kinetics in Nb-microalloyed TRIP steels with increased Mn content. *Adv. Mater. Res.* **2011**, *314–316*, 119–122. [[CrossRef](#)]
4. Dobrzanski, L.A.; Borek, W. Hot-working behaviour of advanced high-manganese C-Mn-Si-Al steels. *Mater. Sci. Forum* **2010**, *654–656*, 266–269. [[CrossRef](#)]
5. Jablonska, M.B. Mechanical properties and fractographic analysis of high manganese steels after dynamic deformation tests. *Arch. Metall. Mater.* **2014**, *59*, 1193–1197. [[CrossRef](#)]
6. Steineder, K.; Schneider, R.; Krizan, D.; Beal, C.; Sommitsch, C. Investigation on the microstructural evolution in a medium-Mn steel (X10Mn5) after intercritical annealing. *HTM J. Heat Treat. Mater.* **2015**, *70*, 19–25. [[CrossRef](#)]
7. Kowalska, J.; Ratuszek, W.; Witkowska, M.; Zielińska-Lipiec, A.; Kowalski, M. Microstructure and texture evolution during cold-rolling in the Fe-23Mn-3Si-3Al alloy. *Arch. Metall. Mater.* **2015**, *60*, 1789–1794. [[CrossRef](#)]
8. Grajcar, A.; Kciuk, M.; Topolska, S.; Plachcinska, A. Microstructure and corrosion behavior of hot-deformed and cold-strained high-Mn steels. *J. Mater. Eng. Perform.* **2016**, *25*, 2245–2254. [[CrossRef](#)]
9. Kucerova, L.; Opatova, K.; Kana, J.; Jirkova, H. High versatility of niobium and alloyed AHSS. *Arch. Metall. Mater.* **2017**, *62*, 1485–1491. [[CrossRef](#)]
10. Tehovnik, F.; Steiner-Petrovic, D.; Vode, F.; Burja, J. Influence of molybdenum on the hot-tensile properties of austenitic stainless steels. *Mater. Tehnol.* **2012**, *6*, 649–655.
11. Radwanski, K. Application of FEG-SEM and EBSD methods for the analysis of the restoration processes occurring during continuous annealing of Dual-Phase steel strips. *Steel Res. Int.* **2015**, *86*, 1379–1390. [[CrossRef](#)]
12. Mazancova, E.; Mazanec, K. The stacking fault energy evaluation of the TWIP and TRIPLEX alloys. *Kovove Mater.* **2009**, *47*, 353–358.
13. Grajcar, A.; Plachcinska, A.; Topolska, S.; Kciuk, M. Effect of thermomechanical treatment on the corrosion behavior of Si and Al-containing high-Mn austenitic steel with Nb and Ti microaddition. *Mater. Tehnol.* **2015**, *49*, 889–894. [[CrossRef](#)]
14. Gorka, J. Microstructure and properties of the high-temperature (HAZ) of thermo-mechanically treated S700MC high-yield-strength steel. *Mater. Tehnol.* **2016**, *50*, 617–621. [[CrossRef](#)]
15. Kurc-Lisiecka, A.; Lisiecki, A. Laser welding of the new grade of advanced high-strength steel Domex 960. *Mater. Tehnol.* **2017**, *51*, 199–204. [[CrossRef](#)]
16. Gutierrez-Urrutia, I.; Raabe, D. Grain size effect on strain hardening in twinning-induced plasticity steels. *Scr. Mater.* **2012**, *66*, 992–996. [[CrossRef](#)]
17. Yuan, X.; Chen, L.; Zhao, Y.; Di, H.; Zhu, F. Dependence of grain size on mechanical properties and microstructures of high manganese austenitic steel. *Proc. Eng.* **2014**, *81*, 143–148. [[CrossRef](#)]
18. Dini, G.; Najafizadeh, A.; Ueji, R.; Monir-Vaghefi, S.M. Tensile deformation behavior of high manganese austenitic steel: The role of grain size. *Mater. Des.* **2010**, *31*, 3395–3402. [[CrossRef](#)]
19. Ma, P.; Qian, L.; Meng, J.; Liu, S.; Zhang, F. Fatigue crack growth behavior of a coarse- and a fine-grained high manganese austenitic twin-induced plasticity steel. *Mater. Sci. Eng. A* **2014**, *605*, 160–166. [[CrossRef](#)]
20. Park, K.T.; Jin, K.G.; Han, S.H.; Hwang, S.W.; Choi, K.; Lee, C.S. Stacking fault energy and plastic deformation of fully austenitic high manganese steels: Effect of Al addition. *Mater. Sci. Eng. A* **2010**, *527*, 3651–3661. [[CrossRef](#)]
21. Peng, X.; Zhu, D.; Hu, Z.; Yi, W.; Liu, H.; Wang, M. Stacking fault energy and tensile deformation behavior of high-carbon twinning-induced plasticity steels: Effect of Cu addition. *Mater. Des.* **2013**, *45*, 518–523. [[CrossRef](#)]
22. Shen, Y.S.; Qiu, C.H.; Wang, L.; Sun, X.; Zhao, X.M.; Zuo, L. Effects of cold rolling on microstructure and mechanical properties of Fe-30Mn-3Si-4Al-0.093C TWIP steel. *Mater. Sci. Eng. A* **2013**, *561*, 329–337. [[CrossRef](#)]
23. Allain, S.; Bouaziz, O.; Chateau, J.P. Thermally activated dislocation dynamics in austenitic FeMnC steels at low homologous temperature. *Scr. Mater.* **2010**, *62*, 500–503. [[CrossRef](#)]
24. Pierce, D.T.; Jiménez, J.A.; Bentley, J.; Raabe, D.; Wittig, J.E. The influence of stacking fault energy on the microstructural and strain hardening evolution of Fe–Mn–Al–Si steels during tensile deformation. *Acta Mater.* **2015**, *100*, 178–190. [[CrossRef](#)]

25. Ding, H.; Ding, H.; Song, D.; Tang, Z.; Yang, P. Strain hardening behavior of TRIP/TWIP steel with 18.8% Mn. *Mater. Sci. Eng. A* **2011**, *528*, 868–873. [[CrossRef](#)]
26. Mazurkiewicz, J. *Structure and Properties of High Manganese MnSiAlNbTi-25-1-3 Steels Increased Store of Cold Plastic Deformation Energy*; International OCSCO World Press, Open Access Library: Gliwice, Poland, 2013.
27. Ghasri-Khouzani, M.; McDermid, J.R. Effect of carbon content on the mechanical properties and microstructural evolution of Fe-22Mn-C steels. *Mater. Sci. Eng. A* **2015**, *621*, 118–127. [[CrossRef](#)]
28. De Cooman, B.C.; Estrin, Y.; Kim, S.K. Twinning-induced plasticity (TWIP) steels. *Acta Mater.* **2018**, *142*, 283–362. [[CrossRef](#)]
29. Wang, S.J.; Jozaghi, T.; Karaman, I.; Arroyave, R.; Chumlyakov, Y.I. Hierarchical evolution and thermal stability of microstructure with deformation twins in 316 stainless steel. *Mater. Sci. Eng. A* **2017**, *694*, 121–131. [[CrossRef](#)]
30. Jiménez, J.A.; Frommeyer, G. Analysis of the microstructure evolution during tensile testing at room temperature of high-manganese austenitic steel. *Mater. Charact.* **2010**, *61*, 221–226. [[CrossRef](#)]
31. Xie, X.; Ninga, D.; Sun, J. Strain-controlled fatigue behavior of cold-drawn type 316 austenitic stainless steel at room temperature. *Mater. Charact.* **2016**, *120*, 195–202. [[CrossRef](#)]
32. Liu, F.; Dan, W.J.; Zhang, W.G. The effects of stress state on the strain hardening behaviors of TWIP steel. *J. Mater. Eng. Perform.* **2017**, *26*, 2721–2728. [[CrossRef](#)]
33. Bouaziz, O.; Guelton, N. Modelling of TWIP effect on work-hardening. *Mater. Sci. Eng. A* **2001**, *319*, 246–249. [[CrossRef](#)]



© 2018 by the authors. Licensee MDPI, Basel, Switzerland. This article is an open access article distributed under the terms and conditions of the Creative Commons Attribution (CC BY) license (<http://creativecommons.org/licenses/by/4.0/>).